

1 Functional MRI brain state 2 occupancy in the presence of 3 cerebral small vessel disease – 4 pre-registration for a replication 5 analysis of the Hamburg City Health 6 Study

✉ For correspondence:
e.schlemm@uke.de

Present address:
Dr. Dr. Eckhard Schlemm,
Klinik und Poliklinik für
Neurologie,
Universitätsklinikum
Hamburg-Eppendorf,
Martinistr. 52,
D-20251 Hamburg

Data availability:
Preprocessed data will be
available e.g. on
<https://github.com/csi-hamburg/HCHS-brain-states-RR>.

Funding: Deutsche
Forschungsgemeinschaft
(DFG) - 178316478 - C2

Competing interests: The
author declares no
competing interests.

7 **Eckhard Schlemm, MBBS PhD^①✉ and Thies Ingwersen, MD¹**

8 ¹Department of Neurology, University Medical Center
9 Hamburg-Eppendorf

11 **Abstract**

12 **Objective:** To replicate recent findings about the association between the extent of
13 cerebral small vessel disease (cSVD), functional brain network dedifferentiation and
14 cognitive impairment.
15 **Methods:** We will analyze demographic, imaging and behavioral data from the
16 prospective population-based Hamburg City Health Study. Using a fully prespecified
17 analysis pipeline, we will estimate discrete brain states from structural and resting-state
18 functional magnetic resonance imaging (MRI). In a multiverse analysis we will vary brain
19 parcellations and functional MRI confound regression strategies. Severity of cSVD will
20 be operationalised as the volume of white matter hyperintensities of presumed
21 vascular origin. Processing speed and executive dysfunction are quantified by the trail
22 making test (TMT).
23 **Hypotheses:** We hypothesize a) that greater volume of supratentorial white matter

²⁴ hyperintensities is associated with less time spent in functional MRI-derived brain
²⁵ states of high fractional occupancy; and b) that less time spent in these high-occupancy
²⁶ brain states is associated with longer time to completion in part B of the TMT.

²⁷

²⁸ Introduction

²⁹ Cerebral small vessel disease (cSVD) is an arteriolopathy of the brain, associated with
³⁰ age and common cardiovascular risk factors (Wardlaw, C. Smith, and Dichgans, 2013).
³¹ cSVD predisposes to ischemic, in particular lacunar, stroke and may lead to cognitive im-
³² pairment and dementia (Cannistraro et al., 2019). Neuroimaging findings in cSVD reflect
³³ its underlying pathology (Wardlaw, Valdés Hernández, and Muñoz-Maniega, 2015) and
³⁴ include white matter hyperintensities (WMH) and lacunes of presumed vascular origin,
³⁵ small subcortical infarcts and microbleeds, enlarged perivascular spaces as well as brain
³⁶ atrophy (Wardlaw, E. E. Smith, et al., 2013). However, the extent of visible cSVD features
³⁷ on magnetic resonance imaging (MRI) is an imperfect predictor of the severity of clini-
³⁸ cal sequelae (Das et al., 2019), and our understanding of the causal mechanisms linking
³⁹ cSVD-associated brain damage to clinical deficits remains limited (Bos et al., 2018).

⁴⁰ Recent efforts have concentrated on exploiting network aspects of the structural (Tu-
⁴¹ ladhar, Dijk, et al., 2016; Tuladhar, Tay, et al., 2020; Lawrence, Zeestraten, et al., 2018)
⁴² and functional (Dey et al., 2016; Schulz et al., 2021) organization of the brain to under-
⁴³ stand the relation between cSVD and clinical deficits in cognition and other domains re-
⁴⁴ liant on distributed processing. Reduced structural network efficiency has repeatedly
⁴⁵ been described as a causal factor in the development of cognitive impairment, in partic-
⁴⁶ ular executive dysfunction and reduced processing speed, in cSVD (Lawrence, Chung,
⁴⁷ et al., 2014; Shen et al., 2020; Reijmer et al., 2016; Prins et al., 2005). Findings with
⁴⁸ respect to functional connectivity results(FC), on the other hand, are more heteroge-
⁴⁹ neous, perhaps due to its limited reproducibility in than their SC counterparts, perhaps
⁵⁰ because FC measurements are prone to be affected by hemodynamic factors and noise,
⁵¹ resulting in relatively low reliability, especially with resting-state scans of short duration
⁵² (Laumann, Gordon, et al., 2015). This problem is exacerbated in the presence of cSVD
⁵³ and dependence on made worse by the arbitrary processing choices (Lawrence, Tozer,
⁵⁴ et al., 2018; Gesierich et al., 2020).

⁵⁵ As a promising new avenue, time-varying, or dynamic, functional connectivity approaches

56 have more recently been explored in patients with subcortical ischemic vascular disease
57 (Yin et al., 2022; Xu et al., 2021). While the study of dynamic FC measures may not
58 solve the problem of limited reliability, especially in small populations or subjects with
59 extensive structural brain changes, it adds another – temporal – dimension to the study of
60 functional brain organisation, which is otherwise overlooked. Importantly, FC dynamics
61 do not only reflect moment-to-moment fluctuations in cognitive processes but are also
62 related to brain plasticity and homeostasis (Laumann and Snyder, 2021; Laumann, Snyder,
63 et al., 2017), which may be impaired in cSVD.

64 In the present paper, we aim to replicate and extend the main results of (Schlemm et
65 al., 2022); in this recent study, the authors analyzed MR imaging and clinical data from the
66 prospective Hamburg City Health Study (HCHS, Jagodzinski et al., 2020) using a coacti-
67 vation pattern approach to define discrete brain states and found associations between
68 the WMH load, time spent in high-occupancy brain states characterized by activation
69 or suppression of the default mode network (DMN) and ~~executive dysfunction~~cognitive
70 impairment.

71 The fractional occupancy of a functional MRI-derived discrete brain state is a subject-specific
72 measure of brain dynamics defined as the proportion of BOLD volumes assigned to that
73 state relative to all BOLD volumes acquired during a resting-state scan.

74 Our primary hypothesis is that the volume of supratentorial white matter hyperinten-
75 sities is associated with the fractional occupancy (~~defined below~~) of DMN-related brain
76 states in a middle-aged to elderly population mildly affected by cSVD. Our second hy-
77 pothesis is that this fractional occupancy is associated with executive dysfunction and
78 reduced processing speed, measured as the time to complete part B of the trail making
79 test (TMT).

80 Both hypotheses will be tested in an independent subsample of the HCHS study popu-
81 lation using the same imaging protocols, examination procedures and analysis pipelines
82 as in (Schlemm et al., 2022). The robustness of associations will be explored in a multi-
83 verse approach by varying key steps in the analysis pipeline.

84 Methods

85 Study population

86 The paper will analyze data from the Hamburg City Health Study (HCHS), which is an
87 ongoing prospective, population-based cohort study aiming to recruit a cross-sectional

Question	Hypothesis	Sampling plan	Analysis plan	Rationale deciding sensitivity for the test	Interpretation given different outcomes	Theory that could be shown wrong by the outcome
Is severity of cerebral small vessel disease, quantified by the volume <u>of</u> supratentorial white matter hyperintensities of presumed vascular origin (WMH), associated with time spent in high-occupancy brain states, defined by resting-state functional MRI	Higher WMH volume is associated with lower average occupancy of the two highest-occupancy brain states.	Available subjects with clinical and imaging data from the <u>the</u> HCHS (Jagodzinski et al., 2020)	Standardized preprocessing of structural and functional MRI data • automatic quantification of WMH • co-activation pattern analysis • multivariable generalised regression analyses	Tradition	$P < 0.05 \rightarrow$ rejection of the null hypothesis of no association between cSVD and fractional occupancy; $P > 0.05 \rightarrow$ insufficient evidence to reject the null hypothesis	Functional brain dynamics are not related to subcortical ischemic vascular disease.

Table 1. Study Design Template

⁸⁸ sample of 45 000 adult participants from the city of Hamburg, Germany (Jagodzinski et al.,
⁸⁹ 2020). From the first 10 000 participants of the HCHS we will aim to include those who
⁹⁰ were documented to have received brain imaging ($n=2652$) and exclude those who were
⁹¹ analyzed in our previous report (Schlemm et al., 2022) ($n=988$, for an expected sample
⁹² size of approximately 1500 participants). The ethical review board of the Landesärztekam-
⁹³ mer Hamburg (State of Hamburg Chamber of Medical Practitioners) approved the HCHS
⁹⁴ (PV5131), all participants provided written informed consent.

⁹⁵ Demographic and clinical characterization

⁹⁶ From the study database we will extract participants' age at the time of inclusion in years,
⁹⁷ their self-reported gender and the number of years spent in education. During the visit
⁹⁸ at the study center, participants undergo cognitive assessment using standardized tests.
⁹⁹ We will extract from the database their performance scores in the Trail Making Test part
¹⁰⁰ B, measured in seconds, as an operationalization of executive function and psychomotor
¹⁰¹ processing speed (Tombaugh, 2004; Arbuthnott and Frank, 2000).

¹⁰² MRI acquisition and preprocessing

¹⁰³ The magnetic resonance imaging protocol for the HCHS includes structural and resting-
¹⁰⁴ state functional sequences. The acquisition parameters on a 3 T Siemens Skyra MRI scan-
¹⁰⁵ ner (Siemens, Erlangen, Germany) have been reported before (Petersen et al., 2020; Frey
¹⁰⁶ et al., 2021) and are given as follows:

¹⁰⁷ For T_1 -weighted anatomical images, a 3D rapid acquisition gradient-echo sequence
¹⁰⁸ (MPRAGE) was used with the following sequence parameters: repetition-repetition time
¹⁰⁹ TR = 2500 ms, echo time TE = 2.12 ms, 256 axial slices, slice thickness ST = 0.94 mm, and
¹¹⁰ in-plane resolution IPR = $(0.83 \times 0.83) \text{ mm}^2$.

¹¹¹ T_2 -weighted fluid attenuated inversion recovery (FLAIR) images were acquired with
¹¹² the following sequence parameters: TR = 4700 ms, TE = 392 ms, 192 axial slices, ST =
¹¹³ 0.9 mm, IPR = (0.75×0.75) mm².

¹¹⁴ 125 resting state functional MRI volumes were acquired (TR = 2500 ms; TE = 25 ms;
¹¹⁵ flip angle = 90°; slices = 49; ST = 3 mm; slice gap = 0 mm; IPR = (2.66×2.66) mm²). Subjects
¹¹⁶ were asked to keep their eyes open and to think of nothing.

¹¹⁷ We will verify the presence and voxel-dimensions of expected MRI data for each par-
¹¹⁸ ticipant and exclude those for whom at least one of T_1 -weighted, FLAIR and resting-state
¹¹⁹ MRI is missing. We will also exclude participants with a neuroradiologically confirmed
¹²⁰ space-occupying intra-axial lesion. To ensure reproducibility, no visual quality assess-
¹²¹ ment on raw images will be performed.

¹²² For the remaining participants, structural and resting-state functional MRI data will
¹²³ be preprocessed using FreeSurfer v6.0 (<https://surfer.nmr.mgh.harvard.edu/>), and fmriPrep
¹²⁴ v20.2.6 (Esteban et al., 2019), using default parameters. Participants will be excluded if
¹²⁵ automated processing using at least one of these packages fails.

¹²⁶ Quantification of WMH load

¹²⁷ For our primary analysis, the extent of ischemic white matter disease will be operational-
¹²⁸ ized as the total volume of supratentorial WMHs obtained from automated segmentation
¹²⁹ using a combination of anatomical priors, BIANCA (Griffanti, Zamboni, et al., 2016) and
¹³⁰ LOCATE (Sundaresan et al., 2019), post-processed with a minimum cluster size of 30 vox-
¹³¹ els, as described in (Schlemm et al., 2022). In an exploratory analysis, we partition voxels
¹³² identified as WMH into deep and periventricular components according to their distance
¹³³ to the ventricular system (cut-off 10 mm, (Griffanti, Jenkinson, et al., 2018))

¹³⁴ Brain state estimation

¹³⁵ Output from fMRIprep will be post-processed using xcpEngine v1.2.1 to obtain de-confounded
¹³⁶ spatially averaged BOLD time series (Circi, Wolf, et al., 2017). For the primary analysis we
¹³⁷ will use the 36p regression strategy and the Schaefer-400 parcellation (Schaefer et al.,
¹³⁸ 2018), as in (Schlemm et al., 2022).

¹³⁹ Different atlases and confound regression strategies, as implemented in xcpEngine,
¹⁴⁰ will be included in the exploratory multiverse analysis.

¹⁴¹ Co-activation pattern (CAP) analysis will be performed by first aggregating parcellated,
¹⁴² de-confounded BOLD signals into a ($n_{\text{parcels}} \times \sum_i n_{\text{time points},i}$) feature matrix, where $n_{\text{time points},i}$

¹⁴³ denotes the number of retained volumes for subject i after confound regression. Clustering will be performed using the k -means algorithm ($k = 5$) with distance measure given by 1 minus the sample Pearson correlation between points, as implemented in Matlab R2021a. We will estimate subject- and state-specific fractional occupancies, which are defined as the proportion of BOLD volumes assigned to each brain state (Vidaurre et al., 2018). The two states with the highest average occupancy will be identified as the basis for further analysis.

¹⁵⁰ Statistical analysis

¹⁵¹ For demographic (age, gender, years of education) and clinical (TMT-B) variables the number of missing records will be reported. For non-missing values, we will provide descriptive summary statistics using median and interquartile range. The proportion of men and women in the sample will be reported. [Regression modelling will be carried out as a complete-case analysis.](#)

¹⁵⁶ As a first outcome-neutral quality check of the implementation of the MRI processing pipeline, brain state estimation and co-activation pattern analysis, we will compare fractional occupancies between brain states. We expect that the average fractional occupancy in two high-occupancy states is higher than the average fractional occupancy in the other three states. Point estimates and 95% confidence intervals will be presented for the difference in average fractional occupancy to check this assertion.

¹⁶² For further analyses, non-zero WMH volumes will be subjected to a logarithmic transformation. Zero values will retain their value zero; to compensate, all models will include a binary indicator for zero WMH volume if at least one non-zero value is present.

¹⁶⁵ To assess the primary hypothesis of a negative association between the extent of ischaemic white matter disease and time spent in high-occupancy brain states, we will perform a fixed-dispersion beta-regression to model the logit of the conditional expectation of the average fractional occupancy of two high-occupancy states as an affine function of the logarithmized WMH load. Age and gender will be included as covariates. The strength of the association will be quantified as an odds ratio per interquartile ratio of the WMH burden distribution and accompanied by a 95% confidence interval. Significance testing of the null hypothesis of no association will be conducted at the conventional significance level of 0.05. Estimation and testing will be carried out using the 'betareg' package v3.1.4 in R v4.2.1.

¹⁷⁵ To assess the secondary hypothesis of an association between time spent in high-

occupancy brain states and executive dysfunction, we will perform a generalized linear regression with a Gamma response distribution to model the logarithm of the conditional expected completion time in part B of the TMT as an affine function of the average fractional occupancy of two high-occupancy states. Age, gender, years of education and logarithmized WMH load will be included as covariates. The strength of the association will be quantified as a multiplicative factor per percentage point and accompanied by a 95% confidence interval. Significance testing of the null hypothesis of no association will be conducted at the conventional significance level of 0.05. Estimation and testing will be carried out using the `glm` function included in the 'stats' package from R v4.2.1.

Sample size calculation is based on ~~the data presented in, where an odds ratio of was reported as the primary~~ an effect size on the odds ratio scale of 0.95, corresponding to ~~an absolute difference in the probability of occupying a DMN-related brain state between the first and third WMH-load quartile of 1.3 percentage points, and between the 5% and 95% percentile of 3.1 percentage points. Approximating half the difference in fractional occupancy of DMN-related states between different task demands (rest vs n-back) in healthy subjects, which was estimated to lie between 6 and 7 percentage points (Cornblath et al., 2020), this value represent a plausible choice for the smallest~~ effect size of ~~interest~~ theoretical and practical interest. It also equals the effect size estimated based ~~on the data presented in~~ (Schlemm et al., 2022).

We used simple bootstrapping to create 10 000 hypothetical datasets of size 200, 400, 600, 800, 900, 910, ..., 1100, 1200, 1400, 1500, 1600. Each dataset was subjected to the estimation procedure described above. For each sample size, the proportion of datasets in which the primary null hypothesis of no association between fractional occupancy and WMH load could be rejected at $\alpha = 0.05$ was computed and is recorded as a power curve in Figure 1.

It is seen that a sample size of 960 would allow replication of the reported effect with a power of 80.2 %. We anticipate a sample size of 1500, which yields a power of 93.9 %.

Multiverse analysis

Both in (Schlemm et al., 2022) and for our primary replication analysis we made certain analytical choices in the ~~operationalisation~~ operationalization of brain states and ischemic white matter disease, namely the use of the 36p confound regression strategy, the Schaefer-400 parcellation and a BIANCA/LOCATE-based WMH segmentation algorithm. ~~If the hypothesized~~ The robustness of the association between WMH burden

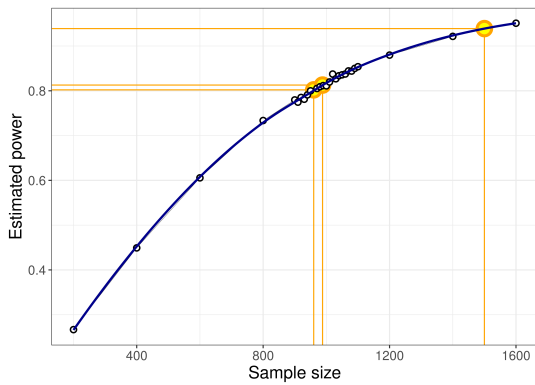


Figure 1. Estimated power for different sample sizes is obtained as the proportion of synthetic data sets in which the null hypothesis of no association between WMH volume and time spent in high-occupancy brain states can be rejected at the $\alpha = 0.05$ significance level. Proportions are based on a total of 10 000 synthetic data sets obtained by bootstrapping the data presented in (Schlemm et al., 2022). Highlighted in orange are the smallest sample size ensuring a power of at least 80 % ($n = 960$), the sample size of the pilot data ($n = 988$, post-hoc power 81.3 %), and the expected sample sample size for this replication study ($n = 1500$, a-priori power 93.9 %).

Name of the atlas	#parcels	Reference
Desikan-Killiany	86	Desikan et al., 2006
AAL	116	Tzourio-Mazoyer et al., 2002
Harvard-Oxford	112	Makris et al., 2006
glasser360	360	Glasser et al., 2016
gordon333	333	Gordon et al., 2016
power264	264	Power, Cohen, et al., 2011
schaefner{N}	100	Schaefer et al., 2018
	200	
	400	

AAL: Automatic Anatomical Labelling

(a) Parcellations

Design	Reference
24p	Friston et al., 1996
24p + GSR	Macey et al., 2004
36p	Satterthwaite et al., 2013
26p-36p + spike regression	Cox, 1996
36p + despiking	Satterthwaite et al., 2013
36p + scrubbing	Power, Mitra, et al., 2014
aCompCor	Muschelli et al., 2014
tCompCor	Behzadi et al., 2007
AROMA	Pruim et al., 2015

GSR: Global signal regression, AROMA: bla
Automatic Removal of Motion Artifacts

(b) Confound regression strategies, adapted from (Circic, Wolf, et al., 2017)

Table 2. Multiverse analysis, implemented using xcpEngine (Circic, Rosen, et al., 2018)

and time spent in high-occupancy states can be replicated using these primary analytical choices, its robustness with regard to other choices will be explored in a multiverse analysis (Steegen et al., 2016). Specifically, in an exploratory analysis, we will estimate brain states from BOLD time series processed according to a variety of established confound regression strategies and aggregated over different cortical brain parcellations (Table 2, Circic, Rosen, et al., 2018; Circic, Wolf, et al., 2017). Extent of cSVD will additionally be quantified by the volume of deep and periventricular white matter hyperintensities.

For each combination of analytical choice of confound regression strategy, parcellation and subdivision of white matter lesion load ($9 \times 9 \times 3 = 243$ scenarios in total) we will quantify the association between WMH load and average time spent in high-occupancy brain states using odds ratio and 95 % confidence intervals as described above.

No hypothesis testing and, therefore, no adjustment for multiple testing, will be

221 carried out in these ~~non-primary analyses~~multiverse analyses. They rather serve to
222 inform about the robustness of the outcome of the test of the primary hypothesis. Any
223 substantial conclusions about the association between severity of cerebral small pathology
224 and time spent in high-occupancy brain states, as stated in the Scientific Question in
225 Table 1, will be drawn from the primary analysis using pre-specified methodological choices.

226

227 ~~Exploratory~~Further exploratory analysis

228 In previous work, two high-occupancy brain states were related to the default-mode net-
229 work (Cornblath et al., 2020). We will further explore this relation by computing, for each
230 individual brain state, the cosine similarity of the positive and negative activations of
231 the cluster's centroid with a set of a-priori defined functional 'communities' or networks
232 (Schaefer et al., 2018; Yeo et al., 2011). Results will be thus visualized as spider plots for
233 the Schaefer, Gordon and Power ~~atlases~~atlases.

234 In further exploratory analyses we plan to describe the associations between brain
235 state dynamics and other measures of cognitive ability, such as memory and language.

236 Code and pilot data

237 Summary data from the first 1000 imaging data points of the HCHS have been published
238 with (Schlemm et al., 2022) and form the basis for the hypotheses tested in this replication
239 study. We have implemented our prespecified analysis pipeline described above in R
240 and Matlab, and applied it to this previous sample. Data, code and results have been
241 stored on GitHub (https://github.com/csi-hamburg/HCHS_brain_states_RR) und preserved
242 on Zenodo.

243 Thus re-analysing data from 988 subjects, the separation between two high-occupancy
244 and three low-occupancy brain states could be reproduced for all combinations of brain
245 parcellation and confound regression strategies (Figure 2).

246 In a multiverse analysis, the main finding was somewhat robust with respect to these
247 choices: a statistically significant negative association between WMH load and time spent
248 in high-occupancy states was observed in 18/81 scenarios, with 5/81 statistically signifi-
249 cant positive associations occurring with the Desikan–Killiany parcellation only (Figure 3).

250 The secondary finding of an association between greater TMT-B times and lower frac-
251 tional occupancy was similarly robust with 12/81 statistically significant negative and no

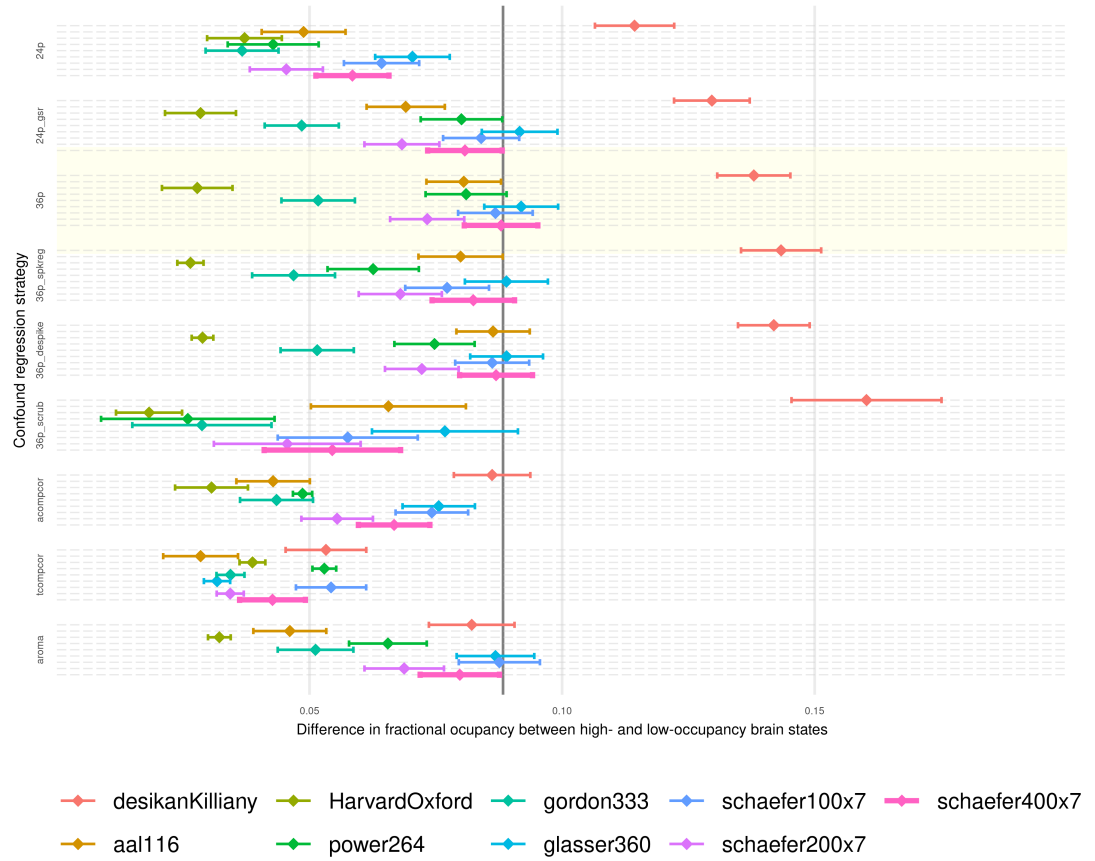


Figure 2. Point estimates (dots) and 95 % confidence intervals (line segments) for the mean difference in fractional occupancy between high- and low occupancy states are shown for different confound regression strategies (groups along the vertical axis) and brain parcellations (color). The difference in FO for a particular choice of regression strategy and brain parcellation is nominally statistically significantly different from zero at a significance level of 5% if the corresponding interval does not contain zero. Hence, the FO difference is significant for all processing choices, reflecting the separation between high- und low-occupancy states. The primary choices (36p and schaefer400) are highlighted by a yellow box and thick pink line, respectively. The effect size reported in (Schlemm et al., 2022) is indicated by a vertical line at 0.08830623.

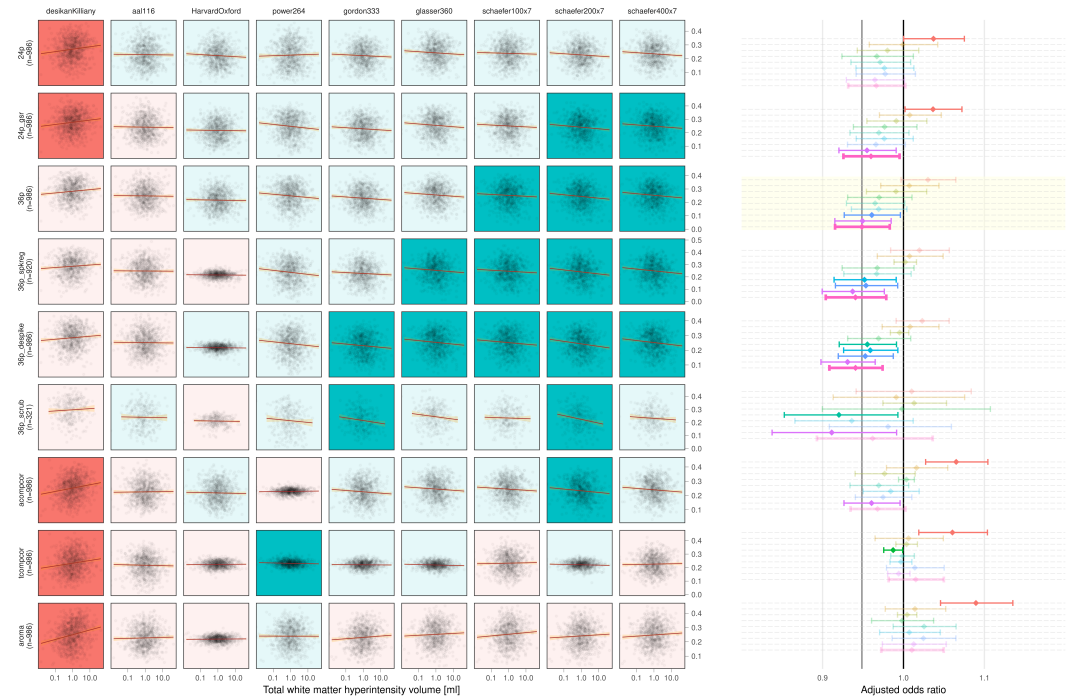


Figure 3. On the left, scatter plots of average fractional occupancies in high-occupancy states against WMH volume on a logarithmic scale (base 10 for easier visualization) for different combinations of confound regression strategies and brain parcellations. Linear regression lines indicate the direction of the unadjusted association between $\log(\text{WMH})$ and occupancy. Background color of individual panels indicates the direction of the association after adjustment for age, sex and zero WMH volume (green, negative; red, positive). A pale background indicates that the association between $\log(\text{WMH})$ and average occupancy is not statistically different from zero. On the right, the same information is shown using point estimates and 95 % confidence intervals for the adjusted odds ratio of the association.

252 statistically significant positive associations.

253 **Timeline and access to data**

254 At the time of planning of this study, all demographic, clinical and imaging data used in
255 this analysis have been collected by the HCHS and are held in the central trial database.
256 Quality checks for non-imaging variables have been performed centrally. WMH segmen-
257 tation based on structural MRI data of the first 10 000 participants of the HCHS has been
258 performed previously using the BIANCA/LOCATE approach (Rimmele et al., 2022) and re-
259 sults are included in this preregistration ([./derivatives/WMH/cSVD_all.csv](#), [./derivatives/WMH/cS](#)).
260 Functional MRI data and clinical measures of executive dysfunction (TMT-B scores) have
261 not been analyzed by the author. Analysis of the data will begin immediately after acceptance-
262 in-principle of the stage 1 submission of the registered report is obtained. Submission
263 of the full manuscript (stage 2) is planned two months later.

264 **Acknowledgment**

265 This preprint was created using the LaPreprint template ([https://github.com/roaldarbol/](https://github.com/roaldarbol/lapreprint)
266 [lapreprint](#)) by Mikkel Roald-Arbøl .

267 **References**

- 268 Arbuthnott, Katherine and Janis Frank (2000). "Trail making test, part B as a measure of
269 executive control: validation using a set-switching paradigm". In: *Journal of clinical and*
270 *experimental neuropsychology* 22.4, pp. 518–528.
- 271 Behzadi, Yashar et al. (2007). "A component based noise correction method (CompCor)
272 for BOLD and perfusion based fMRI". In: *Neuroimage* 37.1, pp. 90–101.
- 273 Bos, Daniel et al. (2018). "Cerebral small vessel disease and the risk of dementia: A sys-
274 tematic review and meta-analysis of population-based evidence". en. In: *Alzheimers.*
275 *Dement.* 14.11, pp. 1482–1492.
- 276 Cannistraro, Rocco J et al. (2019). "CNS small vessel disease: A clinical review". en. In: *Neu-*
277 *rology* 92.24, pp. 1146–1156.
- 278 Ceric, Rastko, Adon FG Rosen, et al. (2018). "Mitigating head motion artifact in functional
279 connectivity MRI". In: *Nature protocols* 13.12, pp. 2801–2826.
- 280 Ceric, Rastko, Daniel H Wolf, et al. (2017). "Benchmarking of participant-level confound
281 regression strategies for the control of motion artifact in studies of functional con-
282 nectivity". en. In: *Neuroimage* 154, pp. 174–187.

- 283 Cornblath, Eli J et al. (2020). "Temporal sequences of brain activity at rest are constrained
284 by white matter structure and modulated by cognitive demands". en. In: *Commun Biol*
285 3.1, p. 261.
- 286 Cox, Robert W (1996). "AFNI: software for analysis and visualization of functional mag-
287 netic resonance neuroimages". In: *Computers and Biomedical research* 29.3, pp. 162–
288 173.
- 289 Das, Alvin S et al. (2019). "Asymptomatic Cerebral Small Vessel Disease: Insights from
290 Population-Based Studies". en. In: *J. Stroke Cerebrovasc. Dis.* 21.2, pp. 121–138.
- 291 Desikan, Rahul S et al. (2006). "An automated labeling system for subdividing the human
292 cerebral cortex on MRI scans into gyral based regions of interest". In: *Neuroimage* 31.3,
293 pp. 968–980.
- 294 Dey, Ayan K et al. (2016). "Pathoconnectomics of cognitive impairment in small vessel
295 disease: A systematic review". en. In: *Alzheimers. Dement.* 12.7, pp. 831–845.
- 296 Esteban, Oscar et al. (2019). "fMRIprep: a robust preprocessing pipeline for functional
297 MRI". en. In: *Nat. Methods* 16.1, pp. 111–116.
- 298 Frey, Benedikt M et al. (2021). "White matter integrity and structural brain network topol-
299 ogy in cerebral small vessel disease: The Hamburg city health study". en. In: *Hum. Brain*
300 *Mapp.* 42.5, pp. 1406–1415.
- 301 Friston, Karl J et al. (1996). "Movement-related effects in fMRI time-series". In: *Magnetic*
302 *resonance in medicine* 35.3, pp. 346–355.
- 303 Gesierich, Benno et al. (2020). "Alterations and test-retest reliability of functional connec-
304 tivity network measures in cerebral small vessel disease". en. In: *Hum. Brain Mapp.*
305 41.10, pp. 2629–2641.
- 306 Glasser, Matthew F et al. (2016). "A multi-modal parcellation of human cerebral cortex".
307 en. In: *Nature* 536.7615, pp. 171–178.
- 308 Gordon, Evan M et al. (2016). "Generation and Evaluation of a Cortical Area Parcellation
309 from Resting-State Correlations". en. In: *Cereb. Cortex* 26.1, pp. 288–303.
- 310 Griffanti, Ludovica, Mark Jenkinson, et al. (2018). "Classification and characterization of
311 periventricular and deep white matter hyperintensities on MRI: A study in older adults".
312 en. In: *Neuroimage* 170, pp. 174–181.
- 313 Griffanti, Ludovica, Giovanna Zamboni, et al. (2016). "BIANCA (Brain Intensity AbNormal-
314 ity Classification Algorithm): A new tool for automated segmentation of white matter
315 hyperintensities". en. In: *Neuroimage* 141, pp. 191–205.

- ³¹⁶ Jagodzinski, Annika et al. (2020). "Rationale and Design of the Hamburg City Health Study".
³¹⁷ en. In: *Eur. J. Epidemiol.* 35.2, pp. 169–181.
- ³¹⁸ Laumann, Timothy O, Evan M Gordon, et al. (2015). "Functional system and areal organi-
³¹⁹ zation of a highly sampled individual human brain". In: *Neuron* 87.3, pp. 657–670.
- ³²⁰ Laumann, Timothy O and Abraham Z Snyder (2021). "Brain activity is not only for thinking".
³²¹ In: *Current Opinion in Behavioral Sciences* 40, pp. 130–136.
- ³²² Laumann, Timothy O, Abraham Z Snyder, et al. (2017). "On the stability of BOLD fMRI
³²³ correlations". In: *Cerebral cortex* 27.10, pp. 4719–4732.
- ³²⁴ Lawrence, Andrew J, Ai Wern Chung, et al. (2014). "Structural network efficiency is as-
³²⁵ sociated with cognitive impairment in small-vessel disease". en. In: *Neurology* 83.4,
³²⁶ pp. 304–311.
- ³²⁷ Lawrence, Andrew J, Daniel J Tozer, et al. (2018). "A comparison of functional and trac-
³²⁸ tography based networks in cerebral small vessel disease". en. In: *Neuroimage Clin* 18,
³²⁹ pp. 425–432.
- ³³⁰ Lawrence, Andrew J, Eva A Zeestraten, et al. (2018). "Longitudinal decline in structural
³³¹ networks predicts dementia in cerebral small vessel disease". en. In: *Neurology* 90.21,
³³² e1898–e1910.
- ³³³ Macey, Paul M et al. (2004). "A method for removal of global effects from fMRI time series".
³³⁴ In: *Neuroimage* 22.1, pp. 360–366.
- ³³⁵ Makris, Nikos et al. (2006). "Decreased volume of left and total anterior insular lobule in
³³⁶ schizophrenia". In: *Schizophrenia research* 83.2-3, pp. 155–171.
- ³³⁷ Muschelli, John et al. (2014). "Reduction of motion-related artifacts in resting state fMRI
³³⁸ using aCompCor". In: *Neuroimage* 96, pp. 22–35.
- ³³⁹ Petersen, Marvin et al. (2020). "Network Localisation of White Matter Damage in Cerebral
³⁴⁰ Small Vessel Disease". en. In: *Sci. Rep.* 10.1, p. 9210.
- ³⁴¹ Power, Jonathan D, Alexander L Cohen, et al. (2011). "Functional network organization of
³⁴² the human brain". en. In: *Neuron* 72.4, pp. 665–678.
- ³⁴³ Power, Jonathan D, Anish Mitra, et al. (2014). "Methods to detect, characterize, and re-
³⁴⁴ move motion artifact in resting state fMRI". In: *Neuroimage* 84, pp. 320–341.
- ³⁴⁵ Prins, Niels D et al. (2005). "Cerebral small-vessel disease and decline in information pro-
³⁴⁶ cessing speed, executive function and memory". en. In: *Brain* 128.Pt 9, pp. 2034–2041.
- ³⁴⁷ Pruim, Raimon HR et al. (2015). "ICA-AROMA: A robust ICA-based strategy for removing
³⁴⁸ motion artifacts from fMRI data". In: *Neuroimage* 112, pp. 267–277.

- 349 Reijmer, Yael D et al. (2016). "Small vessel disease and cognitive impairment: The relevance of central network connections". en. In: *Hum. Brain Mapp.* 37.7, pp. 2446–2454.
- 350
- 351 Rimmele, David Leander et al. (2022). "Association of Carotid Plaque and Flow Velocity With White Matter Integrity in a Middle-aged to Elderly Population". en. In: *Neurology.*
- 352
- 353 Satterthwaite, Theodore D et al. (2013). "An improved framework for confound regression and filtering for control of motion artifact in the preprocessing of resting-state functional connectivity data". In: *Neuroimage* 64, pp. 240–256.
- 354
- 355
- 356 Schaefer, Alexander et al. (2018). "Local-Global Parcellation of the Human Cerebral Cortex from Intrinsic Functional Connectivity MRI". en. In: *Cereb. Cortex* 28.9, pp. 3095–3114.
- 357
- 358 Schlemm, Eckhard et al. (2022). "Equalization of Brain State Occupancy Accompanies Cognitive Impairment in Cerebral Small Vessel Disease". en. In: *Biol. Psychiatry* 92.7, pp. 592–602.
- 359
- 360
- 361 Schulz, Maximilian et al. (2021). "Functional connectivity changes in cerebral small vessel disease - a systematic review of the resting-state MRI literature". en. In: *BMC Med.* 19.1, p. 103.
- 362
- 363
- 364 Shen, Jun et al. (2020). "Network Efficiency Mediates the Relationship Between Vascular Burden and Cognitive Impairment: A Diffusion Tensor Imaging Study in UK Biobank". en. In: *Stroke* 51.6, pp. 1682–1689.
- 365
- 366
- 367 Steegen, Sara et al. (2016). "Increasing Transparency Through a Multiverse Analysis". en. In: *Perspect. Psychol. Sci.* 11.5, pp. 702–712.
- 368
- 369 Sundaresan, Vaanathi et al. (2019). "Automated lesion segmentation with BIANCA: Impact of population-level features, classification algorithm and locally adaptive thresholding". en. In: *Neuroimage* 202, p. 116056.
- 370
- 371
- 372 Tombaugh, Tom N (2004). "Trail Making Test A and B: normative data stratified by age and education". en. In: *Arch. Clin. Neuropsychol.* 19.2, pp. 203–214.
- 373
- 374 Tuladhar, Anil M, Ewoud van Dijk, et al. (2016). "Structural network connectivity and cognition in cerebral small vessel disease". en. In: *Hum. Brain Mapp.* 37.1, pp. 300–310.
- 375
- 376 Tuladhar, Anil M, Jonathan Tay, et al. (2020). "Structural network changes in cerebral small vessel disease". en. In: *J. Neurol. Neurosurg. Psychiatry* 91.2, pp. 196–203.
- 377
- 378 Tzourio-Mazoyer, Nathalie et al. (2002). "Automated anatomical labeling of activations in SPM using a macroscopic anatomical parcellation of the MNI MRI single-subject brain".
- 379
- 380 In: *Neuroimage* 15.1, pp. 273–289.

- ³⁸¹ Vidaurre, Diego et al. (2018). "Discovering dynamic brain networks from big data in rest
³⁸² and task". en. In: *Neuroimage* 180.Pt B, pp. 646–656.
- ³⁸³ Wardlaw, Joanna M, Colin Smith, and Martin Dichgans (2013). "Mechanisms of sporadic
³⁸⁴ cerebral small vessel disease: insights from neuroimaging". en. In: *Lancet Neurol.* 12.5,
³⁸⁵ pp. 483–497.
- ³⁸⁶ Wardlaw, Joanna M, Eric E Smith, et al. (2013). "Neuroimaging standards for research
³⁸⁷ into small vessel disease and its contribution to ageing and neurodegeneration". en.
³⁸⁸ In: *Lancet Neurol.* 12.8, pp. 822–838.
- ³⁸⁹ Wardlaw, Joanna M, María C Valdés Hernández, and Susana Muñoz-Maniega (2015). "What
³⁹⁰ are white matter hyperintensities made of? Relevance to vascular cognitive impairment". en. In: *J. Am. Heart Assoc.* 4.6, p. 001140.
- ³⁹² Xu, Yuanhang et al. (2021). "Altered Dynamic Functional Connectivity in Subcortical Is-
³⁹³ chemic Vascular Disease With Cognitive Impairment". en. In: *Front. Aging Neurosci.* 13,
³⁹⁴ p. 758137.
- ³⁹⁵ Yeo, B T Thomas et al. (2011). "The organization of the human cerebral cortex estimated
³⁹⁶ by intrinsic functional connectivity". en. In: *J. Neurophysiol.* 106.3, pp. 1125–1165.
- ³⁹⁷ Yin, Wenwen et al. (2022). "The Clustering Analysis of Time Properties in Patients With
³⁹⁸ Cerebral Small Vessel Disease: A Dynamic Connectivity Study". en. In: *Front. Neurol.*
³⁹⁹ 13, p. 913241.